Accepted Manuscript

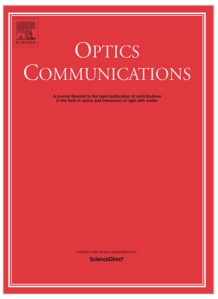

Generation of non-paraxial accelerating beams by active aberration compensation

Yujie Qiu, Xue Mu, Chunmei Zhang, Xiaopei Sun, Yi Hu, Zhigang Chen, Jingjun Xu

PII: S0030-4018(18)31089-7
DOI: https://doi.org/10.1016/j.optcom.2018.12.040
Reference: OPTICS 23708

To appear in: *Optics Communications*

Received date : 19 October 2018
Revised date : 5 December 2018
Accepted date : 9 December 2018

Please cite this article as: Y. Qiu, X. Mu, C. Zhang et al., Generation of non-paraxial accelerating beams by active aberration compensation, *Optics Communications* (2018), https://doi.org/10.1016/j.optcom.2018.12.040

Generation of non-paraxial accelerating beams by active aberration compensation

Yujie Qiu[1], Xue Mu[1], Chunmei Zhang[1], Xiaopei Sun[1], Yi Hu[1*], Zhigang Chen[1,2,3] and Jingjun Xu[1,4]

[1]*The MOE Key Laboratory of Weak-Light Nonlinear Photonics, TEDA Applied Physics Institute and School of Physics, Nankai University, Tianjin 300457, China*

[2]*Department of Physics and Astronomy, San Francisco State University, San Francisco, California 94132, USA*

[3]*Email: zhigang@sfsu.edu*

[4]*Email: jjxu@nankai.edu.cn*

**Corresponding author: yihu@nankai.edu.cn*

Abstract

We demonstrate the generation of non-paraxial accelerating beams by using an objective with an external spherical aberration compensation. A correction phase is applied at an illuminating plane before the objective, and such an aberration-corrected system enables a Fourier transform that translates a proper spatial spectral phase pattern into the desired non-paraxial accelerating beams. The feasibility of the scheme and the quality of the generated beams are further discussed for various conditions. Experimentally, we observe the accelerating beams as well as non-paraxial autofocusing beams following predesigned trajectories generated with such an aberration compensation method, providing an effective and alternative approach for non-paraxial beam shaping.

Keywords: Wave propagation, aberration compensation, invariant optical fields.

1. Introduction

Stemming from the field of quantum mechanics [1], Airy wave-packets that can self-accelerate in free space were introduced into optics in 2007. Since then, self-accelerating Airy beams have attracted a great deal of attention [2-4], triggered by their intriguing propagation properties. They have shown unique features in a

variety of potential applications, such as: particle manipulation [5], curved plasma channel generation [6], light-sheet microscopy [7], and electric discharge guiding [8], to mention just a few.

Limited by the paraxial approximation, Airy beams as well as their circular configurations (namely autofocusing Airy beams [9-11]) are restricted to follow paths with small curvatures. To break this limit, non-paraxial accelerating beams (NABs) were put forward aiming to large bending angles [12-17]. These beams can be generated by using an objective through Fourier-transforming a properly phase-modulated beam [15-17]. Nevertheless, spherical aberration is often introduced in this setup, if the working conditions (such as temperature, light wavelength, coverslip thickness, focal plane depth, refractive index of the environment) deviate from the default values of an objective [18]. In the presence of spherical aberration, light traveling through the periphery of an objective focuses at different positions rather than at the same point. The resulting defocusing effect is detrimental to the realization of a good Fourier transform, hence reducing the quality of the generated NABs. Fortunately, spherical aberration can be compensated by providing a proper phase modulation on the input beam, but thus far such a kind of external aberration correction has not been employed to generate NABs.

In this paper, we demonstrate the generation of NABs by using an objective with an external spherical aberration compensation. Our analysis shows that this system enables a good Fourier transform from the aberration-correction plane to the focal plane, and hence can be employed for producing the NABs. The dependence of the beam quality on the locations of the two planes is further discussed. In experiment, by virtue of the external aberration correction, we achieve optimal generation of the NABs and non-paraxial autofocusing beams that follow several predesigned types of trajectories.

2. Principle of active aberration compensation

In the framework of geometrical optics, a perfect focusing occurs when all the rays passing through an optical system intersect at the same point. This is the prerequisite for a given system to perform a Fourier transformation. However, distortion and defocusing of rays routinely take place in a practical system because of the spherical aberration, among other factors, since a perfect focusing is usually designed for some

unique conditions. Nevertheless, thanks to the external compensation technique, an optimized focusing can be readily recovered for a non-ideal system [19].

We employ a simple yet standard objective that consists of two concavoconvex doublet lens and a third lens (see Table 1 and Fig. 1(a)) to demonstrate our idea. To realize the mentioned focusing, the correction phase (corresponding to the tilts applied on the initially horizontal optical rays in the language of geometrical optics) can be obtained by employing the principle of reversibility of light. In the presence of this correction phase, we test whether such a system follows the translation property of Fourier transform from the correction plane to the focal plane. To this end, a ray emitting from the correction plane is applied by a linear phase modulation αk_x (where α is the modulation depth and k_x is the transverse vector) and its position change (denoted as δ) at the focal plane is recorded. Figure 1(b) presents the value of δ as a function of α for five typical positions at the correction plane (denoted as A, B, C, D and E). Since the points A and B are symmetrical to E and D about the optical axis, respectively, while the point C is on the optical axis, the curves in Fig. 1(b) have central symmetry about the point $(\alpha,\delta) = (0,0)$. The two parameters (α and δ) meet the translation property well for the point C, as can be expected from the paraxial approximation. However, their relationship tends to deviate from the linear case at the peripheral positions, particularly when larger value of $|\alpha|$ is used. For instance, the rays emitting from A and E have larger and smaller shifts compared to the ideal case, respectively, when α is around 0.1 mm. If a slight deviation can be tolerated, Fourier transform is possible under a mild phase modulation depth. We then study how the deviation (denoted by $\Delta\delta$) is influenced by the locations of the correction plane and the focal plane. Figure 1(c) presents the case associated with the point E (a typical periphery position) under a fixed linear phase modulation with α = 0.1 mm (corresponding to δ = 0.1 mm induced by the Fourier transform). One can see that the setting of the correction plane leads to quite small changes on the deviation from δ = 0.1 mm, particularly under the condition of shorter focal lengths. On the other hand, the deviation increases with the focal length. For other points at the correction plane, similar results can be obtained. From the knowledge of the catastrophe theory [20], one should employ an optical system having a larger numerical aperture for realizing NABs with a steeper bending angle. In our study, the value of the numerical aperture is determined by the tilting angle of the outmost rays passing through the focal point,

rather than by the choice of the correction plane. It reaches the maximum at f = ~1.2 mm, as shown in Fig. 1(d). Its reduction upon negative and positive offsets to this focal length is caused by the apertures of the leftmost and rightmost lens respectively. As inferred from the results in Figs. 1(c) and 1(d), it is possible to reach a good condition of Fourier transform while guaranteeing a high numerical aperture for an aberration-corrected objective.

Next, we analyze the caustic for an NAB produced by the aberration-corrected system. As a typical example, an NAB designed to follow a half circle with the radius R = 50 μm is considered and the spectral phase applied is $Rk_x\arcsin(k_x/k)$-Rk_x. The gradient of the phase leads to the tilt of the rays emitting from the correction plane, and it is indeed a k_x-dependent modulation depth α with an expression of $R(k/\sqrt{k^2-k_x^2}-1)$. Thus the value of α is positive for periphery points. Figure 2(a) plots the rays translated by means of geometrical optics in the longitudinal range of the half circle (i.e., 2R). The formed caustics fits well with the target trajectory in most regions, except some deviations near the two ends. Their mismatch is quantified by $\Delta x/R$, where Δx is the difference between the caustic (i.e., the lowest intersection position for the rays passing a vertical plane) and the target trajectory. As can be seen from Fig. 2(b), in most of the acceleration regions, all rays are located above the half circle, but in a region close to the output, some rays distribute off below the designed trajectory. These rays originate from the upper peripheral positions (near E in Fig. 1(a)), and thus have a less upper shift than the ideal case for positive value of α (see the inset in Fig. 1(b)). While for the rays from the lower peripheral positions, the upper shift is larger than the ideal one for positive value of α. Thus no ray is observed to distribute off below the trajectory along the left quadrant. In this study, the longitudinal length of the fitting region is calculated under the condition that the mismatch $\Delta x/R$ is less than 2% (this value is just employed as an example, and the choice of the error is mainly dependent on the requirement in specific applications). The ratio (denoted as γ) between this length and the maximum theoretical acceleration range (i.e., 2R) is used to characterize the proportion of an effective acceleration range. As shown in Fig. 2(c), the value of γ is nearly immune to the setting of the correction plane. On the other hand, it has an optimized value when the focal length is set to be ~1.24 mm, and exhibits a faster decrease for positively offsetting the focal plane relative to the ideal position [Fig. 2(d)]. This can be

interpreted by the result shown in Fig. 1(d) where a similar change versus the focal length exists for the numerical aperture that basically determines the effective acceleration range.

3. Experimental results

To demonstrate the effectiveness of the proposed approach, we perform a series of experiments based on above analysis. Figure 3 presents the schematic of the experimental setup and method. An expanded laser beam (the wavelength is 632.8 nm) is employed to illuminate a programmable spatial light modulator (SLM) with a proper polarization. Using a 4-*f* system (consisting of two lenses with f = 150 mm and f = 100 mm) followed by an objective (×60, numerical aperture is 0.85), the NABs can be produced by imposing proper phases on the SLM. The beam patterns are recorded by an imaging system consisting of another objective and a CCD camera that are placed on the same motorized translation stage.

In general, the objective should work with a coverslip. In order to obtain obvious spherical aberration for the demonstration of our idea, no coverslip is employed in our experiment. Firstly, we correct the aberration in a quasi-one-dimensional (1D) region marked in Fig. 3(b). As expected, the light passing through this area of the objective cannot be perfectly focused without any phase compensation, as shown in Fig. 4(a). To correct the spherical aberration, the liquid crystal panel on the SLM is divided vertically into 36 closely distributed stripes with the same height. For the i^{th} (i = 1 to 18) pair of stripes that are symmetric about the line x=0, a linear phase $\varphi_i(x) = a_i x+by$ and $\varphi_i(x) = -a_i x+by$ (where a_i is the modulation depth and b is a constant) is imposed on the upper and the lower stripe, respectively, while for the other strips, the phase is blank [Fig. 3(c)]. In this way, the beam illuminating the i^{th} pair is separated by the phase term (i.e., the production of b and y) from the major part [Fig. 3(d)], and can be focused to a selected location on the optical axis by the phase term associated with a_i. The value of a_i is carefully chosen to let the separated spot reach the minimum size at the focal plane. Then one can obtain a 1D correction phase, i.e., $\varphi(x)= \Sigma\varphi_i$, to allow a good focusing as shown in Fig. 4(b). Note that since we do not know the parameters of the internal components of the objective, the principle of reversibility of light cannot be used to obtain the correction phase. Although the elements in the objective used in our setup may be different from those in the analysis, we also noticed that

there was an optimized focal length to reach the maximum numerical aperture. In addition, we found that the location of the correction plane did not influence the preformation of the aberration-corrected system.

Before applying the spatial spectral phase (as a function of k_x) of the NABs, k_x is assumed to be linear with the position at the aberration-corrected plane and its spanning is bounded by the tilt of the outermost beams through the formula $k_x = k\sin\theta$, where θ is the angle of the beam about the optical axis. Once the phase term associated with the NABs is applied, the beam can be generated to follow the designed trajectory through the aberration-corrected system. Examples shown in Figs. 4(c-e) are the NABs along circular, parabolic and elliptic paths, respectively. These beams seem to bend less after passing the top of the trajectory compared with the earlier propagation behavior, which is in accord with the analysis presented in Figs. 2(a) and 2(b). In contrast, once the correction phase term is cancelled, the target NAB cannot be produced, as illustrated by an example presented in Fig. 4(f), where the spectral phase used in Fig. 4(c) is imposed alone.

To correct the spherical aberration in two-dimension (2D) region, we simply rotate the 1D correction phase by 180°, considering that our optical system has been aligned to be circularly symmetric about the optical axis. Using the aberration free system, a non-paraxial abruptly autofocusing beam is produced (see Fig. 5). Such a beam initially has a hollow region surrounded by various concentrical rings, and then abruptly focuses to a point at a propagation distance of about 50 μm. The shrinking of its inner ring follows a rate defined by the predesigned circular trajectory $r = (R^2\text{-}z^2)^{1/2}\text{-}0.88R$ (where R = 100 μm), as shown by the side view of the propagation in Fig. 5(e).

4. Conclusion

In conclusion, we have theoretically and experimentally demonstrated that NABs can be generated by employing an objective whose spherical aberration is actively compensated. Our results indicate that the quality of the produced NABs is mainly determined by the choice of the focal plane. Using an aberration-corrected system in this way, both 1D NABs along several types of trajectories and 2D non-paraxial abruptly autofocusing beam are generated. Our method offers a flexible way to produce the NABs in experiment without the necessity to fit an objective to its ideal

working conditions. Hence, our work may prove useful for experimental realization of other kinds of NABs including micro-scale optical bottle beams [21-24] for various applications.

Acknowledgments

National Natural Science Foundation of China (NSFC) (11504186, 61575098, 91750204), the National Key R&D Program of China (2017YFA0303800), the 111 Project in China (B07013).

References

1. M.V. Berry, N.L. Balazs, Nonspreading wave packets, Am. J. Phys. 47 (1979) 264-267.
2. G.A. Siviloglou, J. Broky, A. Dogariu, D.N. Christodoulides, Observation of accelerating Airy beams, Phys. Rev. Lett. 99 (2007) 213901.
3. G.A. Siviloglou, D.N. Christodoulides, Accelerating finite energy Airy beams, Opt. Lett. 32 (2007) 979-981.
4. Y. Hu, G.A. Siviloglou, P. Zhang, N.K. Efremidis, D.N. Christodoulides, Z. Chen, Self-Accelerating Airy Beams: Generation, Control, and Applications, in Nonlinear Photonics and Novel Optical Phenomena, Z. Chen, R. Morandotti, eds. 170 (Springer, 2012) 1–46.
5. J. Baumgartl, M. Mazilu, K. Dholakia, Optically mediated particle clearing using Airy wavepackets, Nat. Photonics 2 (2008) 675-678.
6. P. Polynkin, M. Kolesik, J.V. Moloney, G.A. Siviloglou, D.N. Christodoulides, Curved Plasma Channel Generation Using Ultraintense Airy Beams, Science 324 (2009) 229-232.
7. T. Vettenburg, H.I. Dalgarno, J. Nylk, C. Coll-Lladó, D.E. Ferrier, T. Čižmár, F.J. Gunn-Moore, K. Dholakia, Light-sheet microscopy using an Airy beam, Nat. Methods 11 (2014) 541-544.
8. M. Clerici, Y. Hu, P. Lassonde, C. Milián, A. Couairon, D.N. Christodoulides, Z. Chen, L. Razzari, F. Vidal, F. Légaré, D. Faccio, R. Morandotti, Laser-assisted guiding of electric discharges around objects, Sci. Adv. 1 (2015) e1400111.
9. N.K. Efremidis, D.N. Christodoulides, Abruptly autofocusing waves, Opt. Lett. 35 (2010) 4045-4047.

10. P. Zhang, J. Prakash, Z. Zhang, M.S. Mills, N.K. Efremidis, D.N. Christodoulides, Z. Chen, Trapping and guiding microparticles with morphing autofocusing Airy beams, Opt. Lett. 36 (2011) 2883-2885.
11. D.G. Papazoglou, N.K. Efremidis, D.N. Christodoulides, S. Tzortzakis, Observation of abruptly autofocusing waves, Opt. Lett. 36 (2011) 1842-1844.
12. I. Kaminer, R. Bekenstein, J. Nemirovsky, M. Segev, Nondiffracting accelerating wave packets of Maxwell's equations, Phys. Rev. Lett. 108 (2012) 163901.
13. F. Courvoisier, A. Mathis, L. Froehly, R. Giust, L. Furfaro, P.A. Lacourt, M. Jacquot, J.M. Dudley, Sending femtosecond pulses in circles: highly nonparaxial accelerating beams, Opt. Lett. 37 (2012) 1736-1738.
14. M.A. Bandres, B.M. Rodríguez-Lara, Nondiffracting accelerating waves: Weber waves and parabolic momentum, New J. Phys. 15 (2013) 013054.
15. P. Aleahmad, M.A. Miri, M.S. Mills, I. Kaminer, M. Segev, D.N. Christodoulides, Fully vectorial accelerating diffraction-free Helmholtz beams, Phys. Rev. Lett. 109 (2012) 203902.
16. P. Zhang, Y. Hu, T. Li, D. Cannan, X. Yin, R. Morandotti, Z. Chen, X. Zhang, Nonparaxial Mathieu and Weber accelerating beams, Phys. Rev. Lett. 109 (2012) 193901.
17. A. Mathis, F. Courvoisier, R. Giust, L. Furfaro, M. Jacquot, L. Froehly, J.M. Dudley, Arbitrary nonparaxial accelerating periodic beams and spherical shaping of light, Opt. Lett. 38 (2013) 2218-2220.
18. T.J. Lambert, J.C. Waters, Navigating challenges in the application of superresolution microscopy, J. Cell Biol. 216 (2017) 53-63.
19. T. Čižmár, M. Mazilu, K. Dholakia, In situ wavefront correction and its application to micromanipulation, Nat. Photonics 4 (2010) 388-394.
20. L. Froehly, F. Courvoisier, A. Mathis, M. Jacquot, L. Furfaro, R. Giust, P.A. Lacourt, J. M. Dudley, Arbitrary accelerating micron-scale caustic beams in two and three dimensions, Opt. Express 19 (2011) 16455-16465.
21. I.D. Chremmos, N.K. Efremidis, Nonparaxial accelerating Bessel-like beams, Phys. Rev. A 88 (2013) 063816.
22. Y. Yang, S. Yan, X. Yu, M. Li, B. Yao, Accelerating incoherent hollow beams beyond the paraxial regime, Opt. Express 24 (2016) 27683-27690.

23. R.S. Penciu, Y. Qiu, M. Goutsoulas, X. Sun, Y. Hu, J. Xu, Z. Chen, N.K. Efremidis, Observation of microscale nonparaxial optical bottle beams, Opt. Lett. 43 (2018) 3878-3881.

24. Y. Hu, D. Bongiovanni, Z. Chen, R. Morandotti, Multipath multicomponent self-accelerating beams through spectrum-engineered position mapping, Phys. Rev. A 88 (2013) 043809.

List of Figure captions

Table 1. The parameters (including the radius of curvature and the refractive index) associated with the two concavoconvex doublet lens and the single lens as illustrated in Fig. 1(a).

Fig. 1. (a) Configuration of the objective under test and its intrinsic spherical aberration is compensated by imposing a proper phase correction at $z = 0$; (b) the shifts of rays at the focal plane by applying a test linear phase modulation at the five points marked in (a); (c, d) plot the deviation from the ideal shift (i.e., 0.1 mm) for the case of the E points under a fixed linear phase modulation with $\alpha = 0.1$ mm and numerical aperture (NA), respectively, for various settings of the correction plane and the focal plane. The parameters L and f are defined in Fig. 1(a).

Fig. 2. Analysis of the effective acceleration ranges of an NAB (along a half circle) produced by the aberration-corrected system under test. (a) plots the optical rays (blue) associated with the NAB and the target trajectory (red); (b) the mismatch (defined in the text) between the caustic formed by the rays and the half circle in (a); (c, d) show the parameters to characterize the effective acceleration range for various position settings of the correction plane and the focal plane.

Fig. 3. (a) Illustration of the experimental setup for the generation of NABs with an aberration correction. SLM: spatial light modulator; L: lens; BS: beam splitter; O: objective lens; P: polarizer; M: mirror; CCD: charge coupled device; (b) quasi-1D aberration correction region (blue slashes) marked at the entrance pupil of the target objective (circular blue area). (c) the phase pattern used to make a pair of light to focus at a selected point (i.e., the focal point); (d) the beam pattern at the focal plane with the right and left parts corresponding to the selected pair of light and the remaining beam, respectively.

Fig. 4. Experimental generation of NABs with the method of external aberration correction. (a, b) show the beam focusing scenarios after the objective recorded before and after the use of an aberration compensation, respectively; (c-e) correspond to the generated NABs following a circular, parabolic and elliptic trajectory via the aberration-corrected system; (f) beam propagation under the same condition of (c) but without the correction phase for direct comparison.

Fig. 5. Experimental generation of a non-paraxial autofocusing beam. (a-d): Snapshots of the transverse intensity patterns taken at planes as marked by dashed white lines in (e), where the propagation side-view of the autofocusing beam is presented, and the curved white dashed lines follow part of a circle with the radius being 100 μm.

List of Figures

lens	Radius of curvature (mm)	n
Convex lens (L1)	6	1.5163
Concave lens (L2)	- 6	1.6055
Convex lens (L3)	6	1.5163
Concave lens (L4)	- 6	1.6055
Single lens (L5)	2.3	1.5163

Table. 1

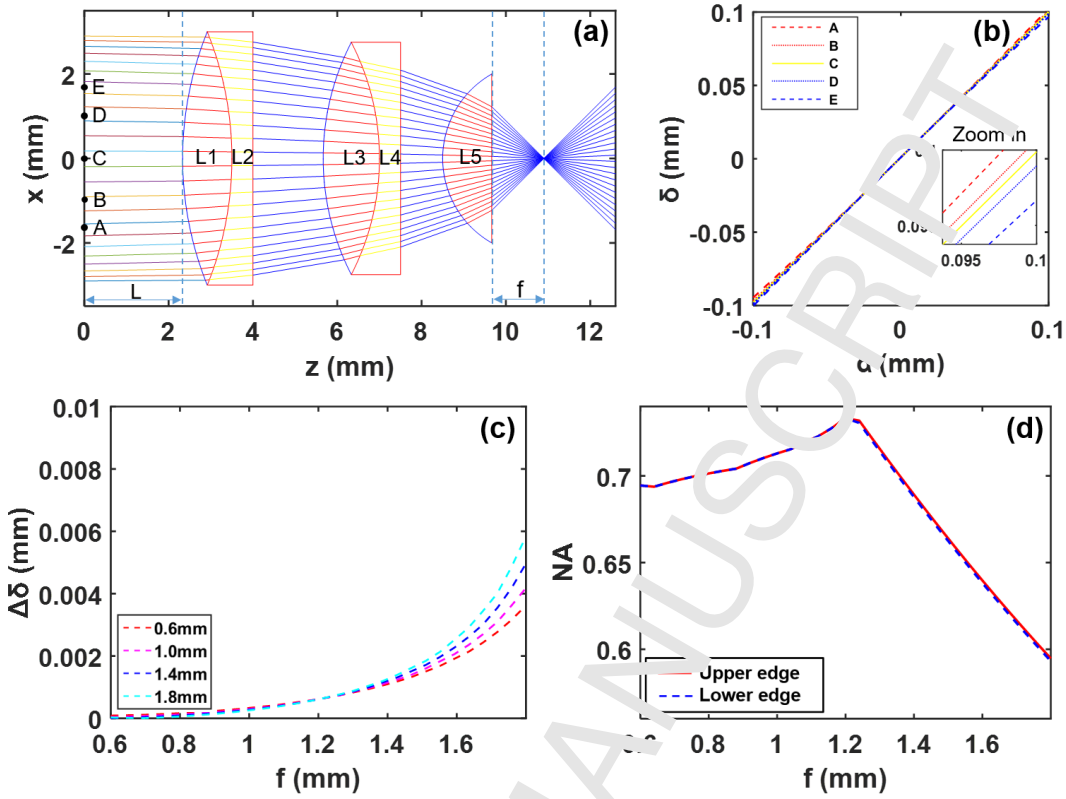

Fig. 1

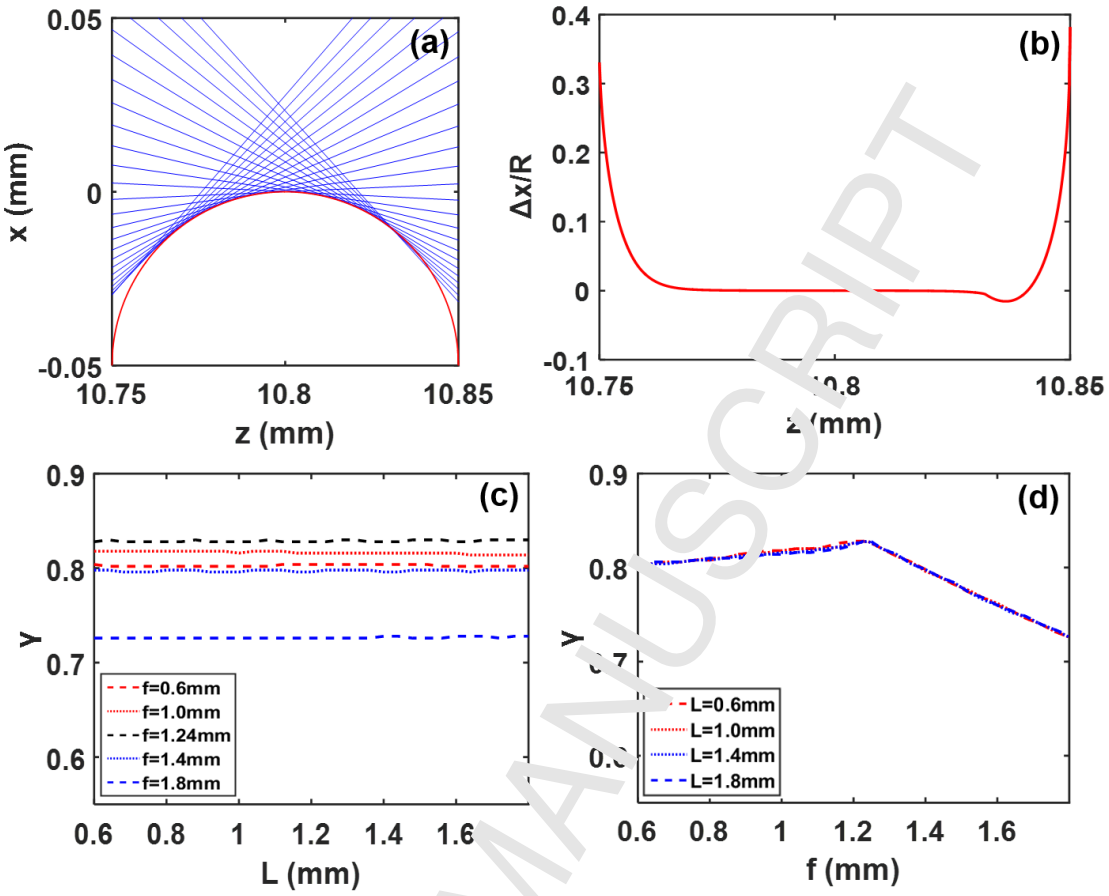

Fig. 2

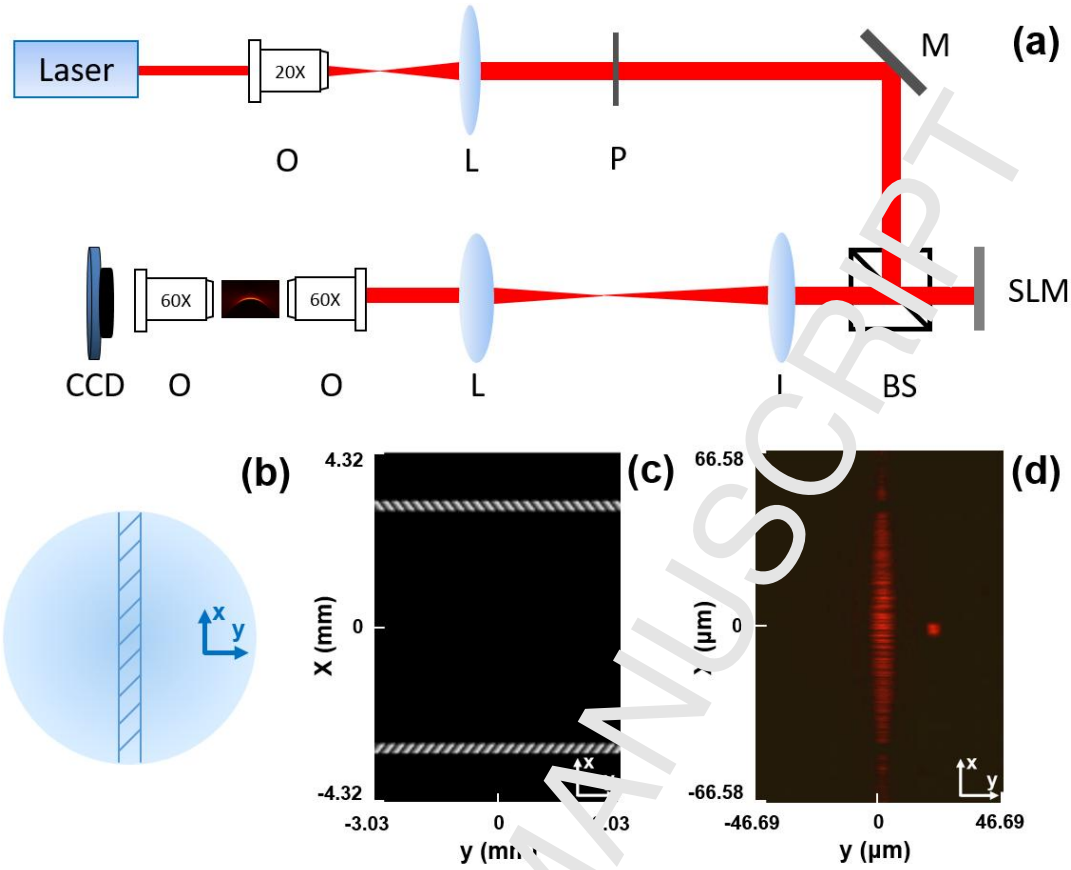

Fig. 3

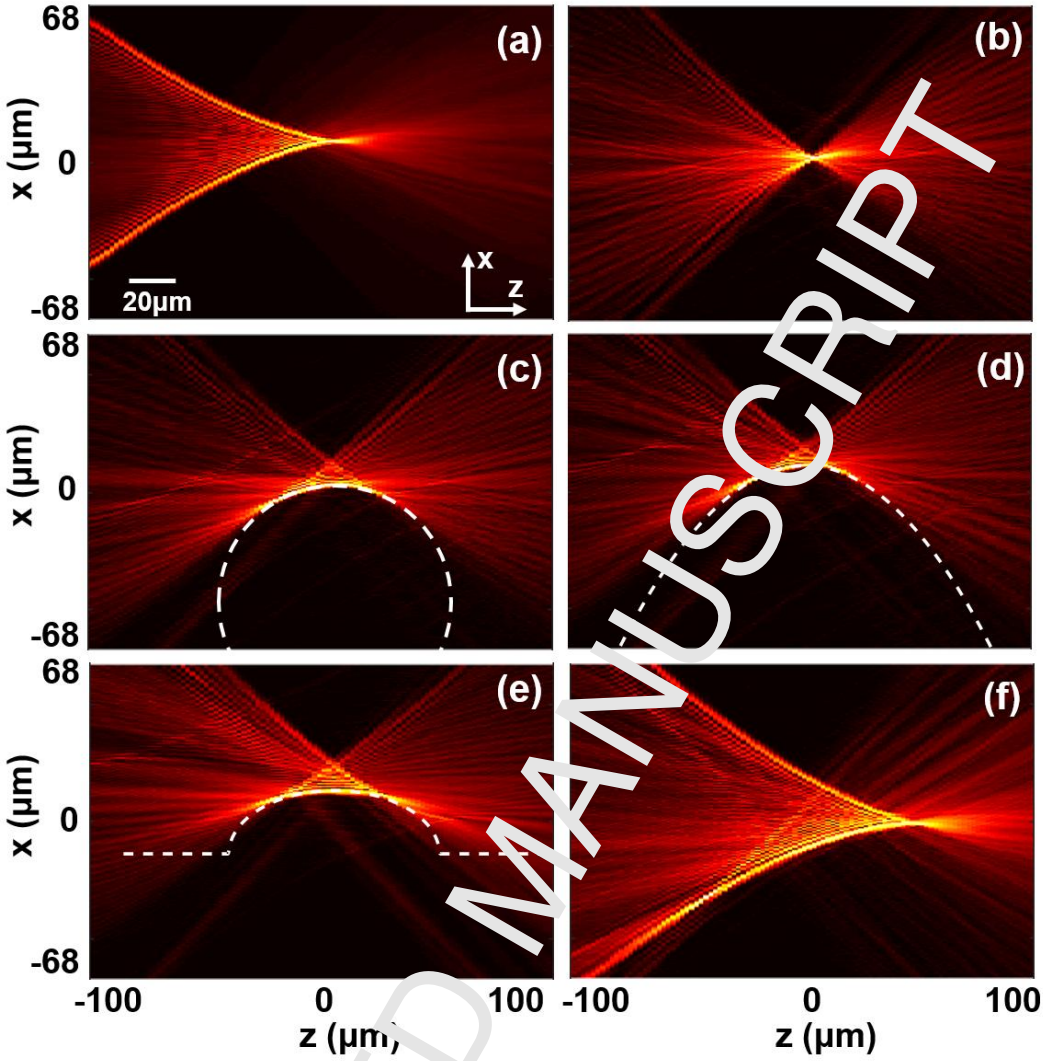

Fig. 4

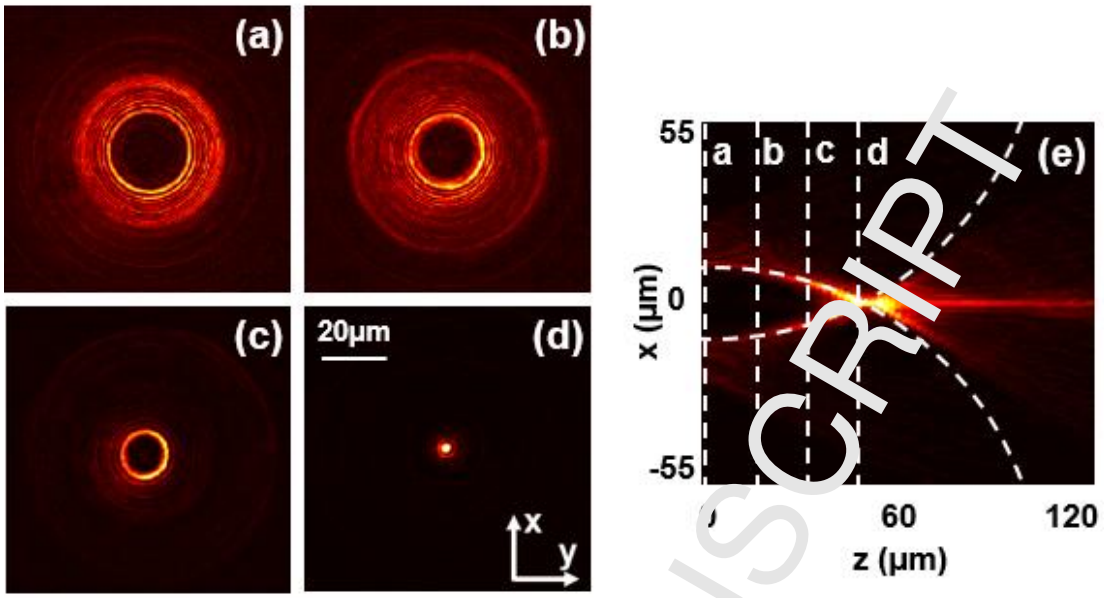

Fig. 5